Supporting Information

Microcapsule functionalization enables rate-determining release from cellulose nonwovens for long-term performance

Viktor Eriksson[a], Jules Mistral[a,b], Ting Yang Nilsson[c], Markus Andersson Trojer[c], and Lars Evenäs[a, d, *]

[a] Department of Chemistry and Chemical Engineering, Chalmers University of Technology, 412 96 Gothenburg, Sweden

[b] Univ Lyon, CNRS, UMR 5223, Ingénierie des Matériaux Polymères, Université Claude Bernard Lyon 1, INSA Lyon, Université Jean Monnet, F-69622 Villeurbanne Cédex, France

[c] Department of Polymers, Fibers and Composites, Fiber Development, RISE, 431 53 Mölndal, Sweden

[d] Wallenberg Wood Science Center, Chalmers University of Technology, 412 96 Gothenburg, Sweden

[*] Corresponding author. E-mail address: lars.evenas@chalmers.se

1. Size distribution

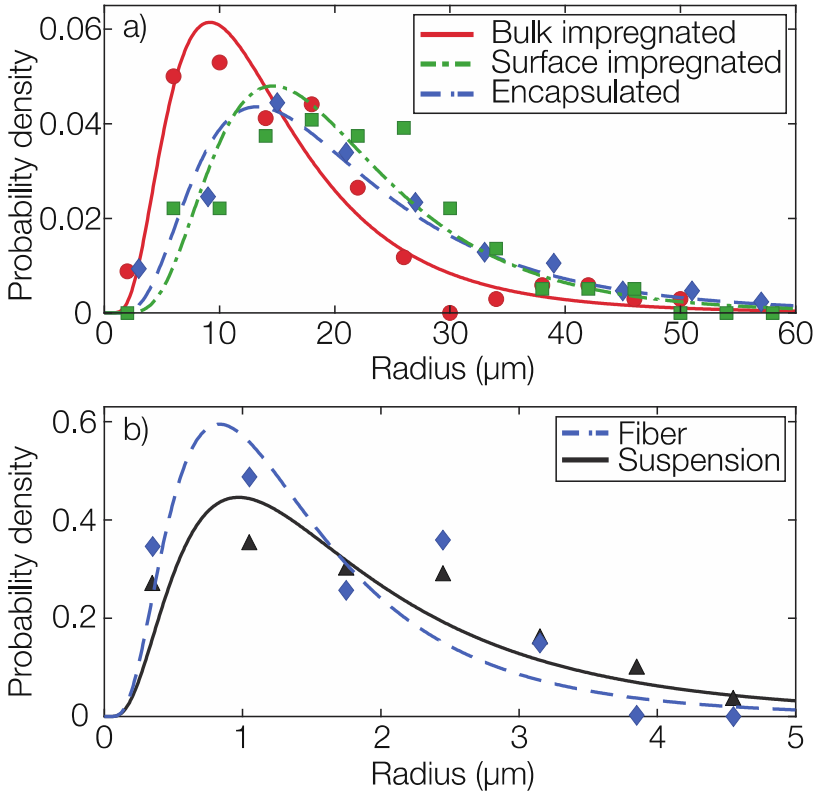

Figure S1. Size distributions of a) the fibers and b) microspheres embedded in fibers and aqueous suspension, respectively.

2. UV-vis spectrophotometry

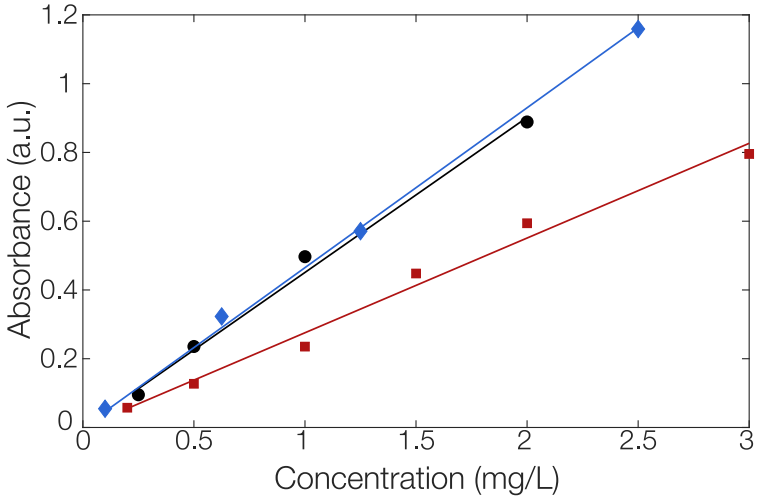

Figure S2. UV-vis calibration curves for pyrene in methanol (●, ε = 0.45 L mg^{-1}cm^{-1}), 3:1 ethanol:6 wt.% (aq.) Brij L23 (♦, ε = 0.47 L mg^{-1}cm^{-1}) and 6 wt.% (aq.) Brij L23 (■, ε = 0.28 L mg^{-1}cm^{-1}).

3. Modelling of pyrene diffusion

The modelling of the diffusional release of pyrene was modelled with the diffusion equations described by Crank.[1] From fibers with bulk impregnated pyrene, the release can be modelled by diffusion from a cylinder with a homogeneous distribution of pyrene. This can be applied to fibers containing microspheres as well, however, this results in an apparent diffusivity across the entire fiber cross-section rather than an effective diffusion coefficient. Similar to a sphere, release from a cylinder can be described by

$$f_c(a,t) = \frac{\alpha_c}{1+\alpha_c}\left(1 - \sum_{n=1}^{\infty} \frac{4\alpha_c(1+\alpha_c)}{4 + 4\alpha_c + \alpha_c^2 q_{c,n}^2} \exp\left(-\frac{D q_{c,n} t}{a^2}\right)\right) \tag{S1}$$

where a is the fiber radius, and α_c is defined as

$$\alpha_c = \frac{V_{sink}}{V_{cyl} K}. \tag{S2}$$

The coefficient $q_{c,n}$ is defined as the n:th non-zero positive root of

$$\alpha_c q_{c,n} J_0(q_{c,n}) + 2J_1(q_{c,n}) = 0 \tag{S3}$$

where J_0 and J_1 are the Bessel functions of the first kind of order 0 and 1 respectively. Since the fibers also are polydisperse, the final fractional release is given by

$$\frac{m_t}{m_{tot}} = \frac{\int f_c(a,t) p(a) a^2 \, da}{\int p(a) a^2 \, da}. \tag{S4}$$

The final geometry is that when pyrene was impregnated on the fiber surface. In this case, two contributions were seen in the release. Partly there was a rapid burst release, and partly a release from a distance L of the average fiber cross-section into which the pyrene had dissolved during the impregnation. The kinetics of the burst was assumed to follow zero-order kinetics. These two contributions can be expressed as

$$\frac{m_t}{m_{tot}} = \begin{cases} p_b k_b t + (1 - p_b) f_w(L,t) & t < t_b \\ p_b k_b t_b + (1 - p_b) f_w(L,t) & t > t_b \end{cases} \tag{S5}$$

where p_b is the burst fraction, k_b is the rate constant for the burst release and t_b is the time during which the burst release occurs. The diffusional contribution $f_p(L,t)$ was taken as diffusion from a plane sheet,

$$f_p(L,t) = 1 - \sum_{n=0}^{\infty} \frac{8}{(2n+1)^2 \pi^2} \exp\left(-\frac{D(2n+1)^2 \pi^2 t}{4L^2}\right). \tag{S6}$$

Individual fits of the diffusion models to each data set are presented in Figure S3.

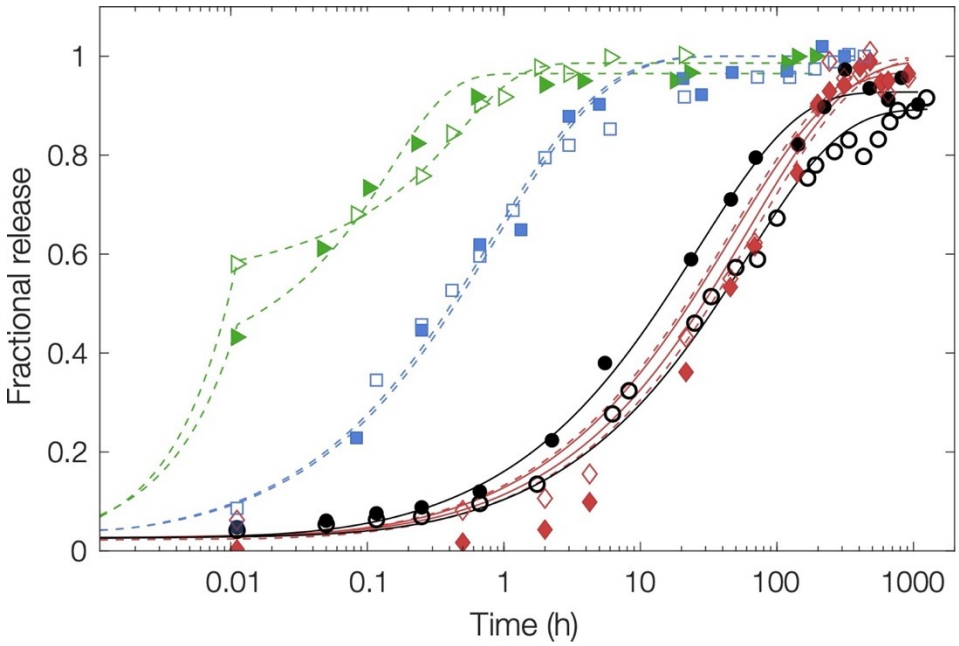

Figure S3. Fractional release from fibers with pyrene loaded by surface impregnation (▷▶□), bulk impregnation (□■), and microencapsulation (◇◆). Release from microspheres in aqueous suspension (○●) is shown as a comparison. Lines represent individual fits of the diffusion equations to each replicate. Solid lines are based on a spherical geometry, and dashed lines are based on a cylindrical geometry.

The specific effect of the microcapsule in terms of barrier properties can be determined by using simplified models[2]. It is important to note here that the models are not intended to predict precise quantities, only the magnitudes of the parameters. These simplifications include steady-state, the reduction to planar geometry (which however is appropriate for sufficiently thin sections at the surface of the microsphere), perfect sink conditions, and a linearization of the concentration gradient in the barrier compartments. The parameters included in the model are defined within a finite fiber segment as visualized in Figure S4.

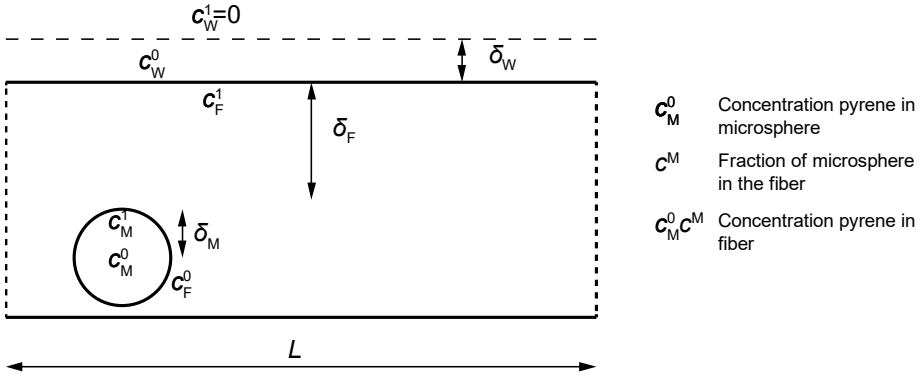

Figure S4. Schematic representation of a fiber segment (index F) containing microspheres (index M) with the parameters used in subsequent models included.

The release rate ($\dot{m}$) can then be expressed as

$$\dot{m} = \frac{A_i D_i \left(c_i^0 - c_i^1\right)}{\delta_i} \qquad \text{(S7)}$$

$$A_{\mathrm{M}}^{\mathrm{TOT}} = \frac{\frac{c^{\mathrm{M}} V_{\mathrm{F}}}{V_{\mathrm{M}}}}{N_{\mathrm{M}}} A_{\mathrm{M}} = \frac{c^{\mathrm{M}} {\delta_{\mathrm{F}}}^2}{\delta_{\mathrm{M}}} \tag{S8}$$

$$A_{\mathrm{F}} = \delta_{\mathrm{F}} L \tag{S9}$$

$$K_{i/j} = \frac{c_i^1}{c_j^0} = \frac{1}{K_{j/i}} \tag{S10}$$

where the indices M denotes the microsphere, F denotes the fiber, and W denotes the aqueous continuous phase. A_i is the surface area for each phase with corresponding diffusion coefficient (D_i) and volume (V_i). Finally, $K_{i/j}$ is the partition coefficient for pyrene between the two phases. At steady state, this leads to

$$\dot{m} = c^{\mathrm{M}} c_{\mathrm{M}}^0 \frac{{\delta_{\mathrm{F}}}^2 L}{\delta_{\mathrm{M}}} \frac{1}{\left(\frac{\delta_{\mathrm{M}}}{D_{\mathrm{M}}} + \frac{\delta_{\mathrm{F}}}{K_{\mathrm{F/M}} D_{\mathrm{F}}} + \underbrace{\frac{\delta_{\mathrm{W}}}{K_{\mathrm{W/M}} D_{\mathrm{W}}}}_{\approx 0} \right)} \tag{S11}$$

The contribution from the diffusive layer in the aqueous phase can be neglected since we can assume that δ_{W} is very small and D_{W} very high.

By defining

$$\dot{m} = \frac{c^{\mathrm{M}} c_{\mathrm{M}}^0 A_{\mathrm{F}}}{\delta_{\mathrm{F}}} D_{\mathrm{app}} \tag{S12}$$

and combining Equation (S11) and (S12), the apparent diffusion coefficient D_{app} can be expressed as

$$D_{\mathrm{app}} = \frac{\delta_{\mathrm{F}}}{\delta_{\mathrm{M}}} \frac{\delta_{\mathrm{F}}}{\left(\underbrace{\frac{\delta_{\mathrm{M}}}{D_{\mathrm{M}}}}_{R_{\mathrm{M}}} + \underbrace{\frac{\delta_{\mathrm{F}}}{K_{\mathrm{F/M}} D_{\mathrm{F}}}}_{R_{\mathrm{F}}} \right)} \tag{S13}$$

Here, the denominator can be identified as the resistance R_i towards diffusion. The ratio δ_F/δ_M is a consequence of the higher total surface area for the microspheres, which for a given c^M increases the release rate as the microsphere radii δ_M decreases. D_M and D_F are the diffusivities of pyrene within each layer, taken from the fitted values in Figure 5 in the article. The partition coefficient $K_{F/M}$ was taken as $K_{F/M} = 0.1$ based on the difference in fluorescence intensity between microcapsule and fiber matrix, respectively, in the confocal micrograph in Figure 2b. A magnification of the confocal micrograph along with an intensity profile across the particle is shown in Figure S5. It should be noted here that part of the fluorescence intensity from the cellulose is due to its autofluorescence, and not necessarily only pyrene. Consequently, the true partition coefficient may be smaller than estimated from micrographs.

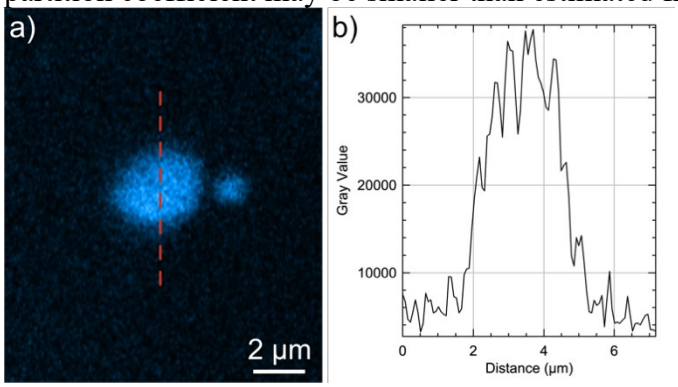

Figure S5. a) Confocal micrograph of a microcapsule embedded in a cellulose fiber. b) Intensity profile along the red dashed line shown in a).

Using the parameters described above, an apparent diffusivity for the composite material of $D_{app} = 3 \cdot 10^{-16}$ m^2s^{-1} was found. This was in excellent agreement with the fitted apparent diffusion coefficient from the solution to the diffusion equation on a cylindrical geometry in Equation S1-S4, see Figure 5 in the article. Moreover, by setting R_M=R_F, it could be determined that the microspheres start to dominate the release already at a critical size δ_M^c of 30 nm. Note that Equation (S13) is not valid for very small δ_M where the area differs considerably between the microspheres and the fiber. Instead, for visualizing the effect of R_i on D_{app}, the areas between all phases can be taken as constant and equal. In this case, Equation (S13) is reduced to

$$D_{app} = \frac{\delta_M + \delta_F}{\frac{\delta_M}{D_M} + \frac{\delta_F}{K_{F/M} D_F}}, \qquad \text{(S14)}$$

which is shown graphically in Figure S6.

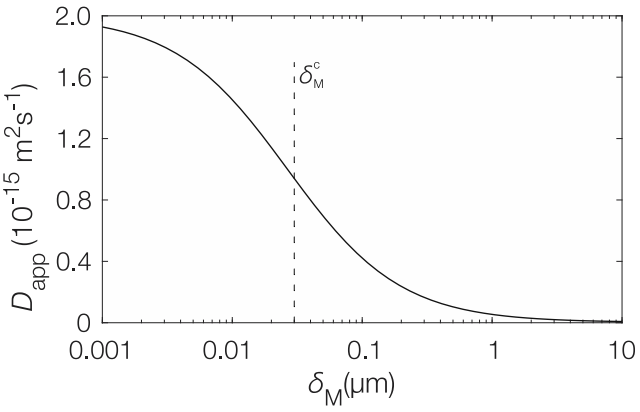

Figure S6. Apparent pyrene diffusivity D_{app} in a composite cellulose fiber containing microspheres of size δ_M, with the critical microsphere size (δ_M^c) marked by a dashed line.

4. Release measurements

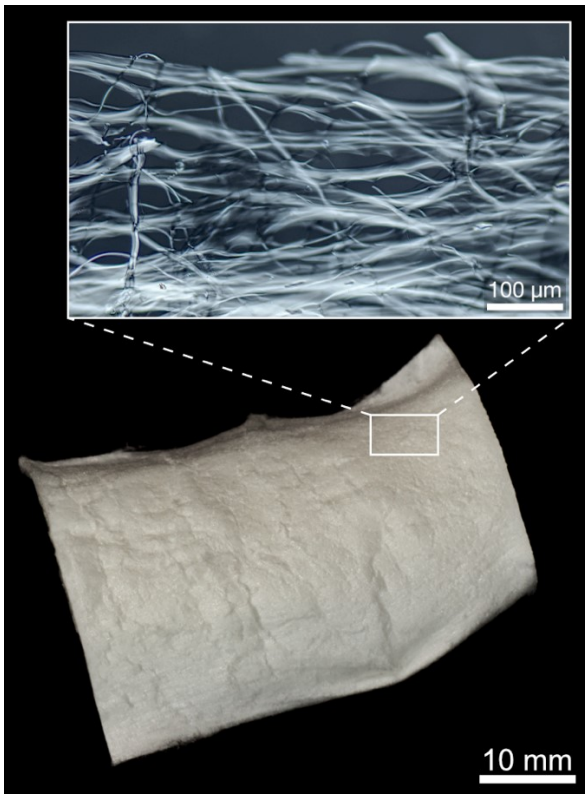

Figure S7. Photograph of a small section of the prepared nonwoven materials. The inset shows a micrograph with a magnification of the fiber structure.

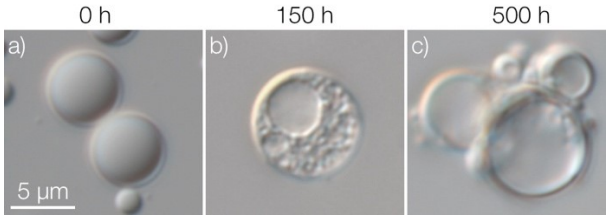

Figure S8. Micrographs of PLGA microcapsules imaged a) immediately after formulation as well as after b) 150 h and c) 500 h in aqueous release medium. The scale bar is valid for all subfigures

In Figure S8, the time-resolved morphological changes of the microcapsules upon hydrolytic degradation are shown. As can be seen, the degradation results in the formation of multiple cavities which after longer times results in a very thin membrane surrounding a large aqueous core. The fact that the cores are aqueous-based can be determined by their transparency (see Figure S8c) and a similar appearance as the background (the same refractive index). Eventually, the entire suspension is rendered completely transparent. None of these changes are clearly visible by inspection of the fiber material containing microcapsules. Confocal microscopy can however reveal that fiber material is in principle void of any active and only the autofluorescence of the cellulose remains (see Figure S9). Note that the microcapsules are hardly discernable in Figure S9. It is worth noting here that the degradation in the fiber material is slower than the corresponding degradation in the aqueous suspension, likely due to the significantly lower exposure to water inside the cellulose matrix.

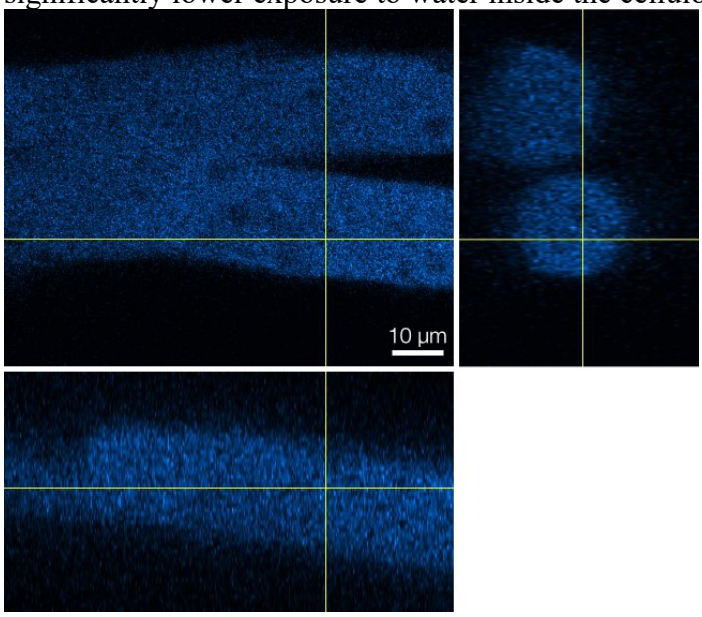

Figure S9. Orthogonal projections of confocal micrographs taken on the microcapsule-loaded material after 2500 hours in the release medium.

5. Cytotoxicity

Table S1. Measured and average absorption of the six replicates of the nonwoven, positive and negative control.

	Absorption (570-650 nm)			Average	Standard deviation
Microsphere-containing nonwoven	0.691	0.680	0.692	0.689	0.007
	0.700	0.687	0.686		
Positive control	0.007	0.008	0.009	0.007	0.002
	0.006	0.005	0.008		
Negative control	0.651	0.660	0.667	0.678	0.022
	0.689	0.700	0.702		

Table S2. Obtained viabilities and cytotoxicity grading as calculated according to ISO10993-5:2009 from the data in Table S1.

	Viability [%]			Average	Standard deviation	Cytotoxicity grading
Microsphere-containing nonwoven	100.7	99.1	100.8	100.5	1.0	Not cytotoxic
	102.0	100.2	100.0			
Positive control	1.0	1.1	1.4	1.0	0.2	Cytotoxic
	0.9	0.7	1.2			
Negative control	94.8	96.2	97.2	98.8	3.2	Not cytotoxic
	100.4	102.0	102.3			

6. References

1. Crank, J., *The mathematics of diffusion*. Oxford university press: 1979.
2. Trojer, M. A.; Andersson, H.; Li, Y.; Borg, J.; Holmberg, K.; Nydén, M.; Nordstierna, L., Charged microcapsules for controlled release of hydrophobic actives. Part III: the effect of polyelectrolyte brush- and multilayers on sustained release. *Physical Chemistry Chemical Physics* **2013,** *15* (17), 6456-6466.